A Rapid 3D fat-water decomposition method using GlObally Optimal Surface Estimation (R-GOOSE)

Chen Cui†, Abhay Shah†, Xiaodong Wu†, Dan Thedens†, Mathews Jacob†

†*Department of Electrical and Computer Engineering, The University of Iowa, Iowa*

June 20, 2017

Correspondence to :

Mathews Jacob,

Department of Electrical and Computer Engineering

3314 Seamans Center

University of Iowa, IA 52242

Email: mathews-jacob@uiowa.edu

Phone: (319) 335-6420

Approximate word count : 2940

Number of figures & tables: 5

Abstract

Purpose: To improve the graph model of our previous work GOOSE for fat-water decomposition with higher computational efficiency and quantitative accuracy.

Methods: A modification of the GOOSE fat water decomposition algorithm is introduced while the global convergence guarantees of GOOSE is still inherited to minimize fat-water swaps and phase wraps. In this paper, two non-equidistant graph optimization frameworks are proposed as a single-step framework termed as rapid GOOSE (R-GOOSE), and a multi-step framework termed as multi-scale rapid GOOSE (mR-GOOSE). Both frameworks contain considerably less graph connectivity than GOOSE, resulting in a great computation reduction thus making it readily applicable to multidimensional fat water applications. The quantitative accuracy and computational time of the novel frameworks are compared with GOOSE on the 2012 ISMRM Challenge datasets to demonstrate the improvement in performance.

Results: Both frameworks accomplish the same level of high accuracy as GOOSE among all datasets. Compared to 100 layers in GOOSE, only 8 layers were used in the new graph model. Computational time is lowered by an order of magnitude to around five seconds for each dataset in (mR-GOOSE), R-GOOSE achieves an average run-time of eight seconds.

Conclusion: The proposed method provides fat-water decomposition results with a lower run-time and higher accuracy compared to the previously proposed GOOSE algorithm.

Key words: 3D fast fat water decomposition, non-equidistant graph model, globally optimal surface search

INTRODUCTION

The separation of water and fat from multi-echo images in MRI is a classic problem with a wide range of important clinical applications (1–3). Since direct methods such as fat saturation (4) and water excitation (5) suffer from their sensitivity to B0 static field inhomogeneity, Dixon based methods have been widely studied because of their robustness to field variations. In the Dixon based model, the estimation of unknown parameters—fat & water components, field inhomogeneity, and T_2^* decay (optional)—is formulated as a nonlinear optimization problem.

The classical approach is to solve the problem at each voxel independently, using either analytical methods (6, 7) or iterative strategies (8). This voxel-by-voxel approach is challenging due to the nonlinearity of the signal model, the ambiguity of the signal model in pixels with only fat or water, and large magnetic field inhomogeneity with high field magnets. The above challenges often result in fat-water swaps and phase wraps in the field inhomogeneity map (1). Various methods have been introduced to address these challenges including region growing (9, 10), region merging (11), iterative graph cut (12), and multi-resolution schemes (13, 14). While these methods provide correct fat-water separations in many applications, they sometimes converge to local minima in difficult cases with large field map variations or low SNR regions such as anatomical cavities which could result in fat-water swaps. Different ingenious strategies such as multi-scale search (15, 16) and region-based labeling (17, 18), have been introduced to minimize the local minima issues and have considerably improved the recovery.

We have previously introduced a non-iterative single-step graph search algorithm termed as GOOSE to estimate the B0 field map as a constrained optimization problem (19). GOOSE minimized the discrete approximation of the original problem, subject to smoothness constraints on the field map. A graph was constructed with as many layers as the size of a uniformly discretized grid, where each node (corresponding to a specific pixel and frequency) is connected to only a few of the nodes in the adjacent pixel within a small range of frequencies. This constrained optimization problem was then solved using a graph search algorithm. The hall-mark of GOOSE was its ability to converge to the global minimum of the GOOSE optimization problem, which follows from (20). The algorithm yielded improved results over many of the state-of-the-art methods such as (9, 10, 12, 14), even though the energy formulation used was simpler than and similar in concept to other formulations. However, a challenge was the high computational complexity that restricted its applicability to large scale 3D problems. In particular, the run-time is dependent on the

graph size, which in turn relies on the discretization of the field map. Typically, the problem discretization creates graphs with more than 100 layers, which results in a computationally expensive algorithm.

In this paper, we introduce computationally efficient extensions of the original GOOSE algorithm, which we term as R-GOOSE and mR-GOOSE, respectively. Specifically, we consider a smoothness penalized likelihood cost function, which is similar in concept to (12, 15). Inspired by (13), we restrict the search at each voxel to a smaller set, specified by the local minima of the voxel independent maximum likelihood cost function. Despite the similarities in the formulation to previous methods, the main novelty of this paper is the graph search algorithm that can account for non-equidistant nodes. Unlike all of the current methods (with the exception of GOOSE), the proposed algorithm is guaranteed to yield the global minimum of the cost function; we note that the minimum may differ from the GOOSE solution since the cost functions are not the same. The global convergence property implies that the quality of fat-water decomposition only depends on the specific cost function. This enables the proposed method to provide a robust decomposition result without using heuristic step such as careful initializations or intermediate steps (multi-resolution etc.) in methods without global optimization guarantees. We also note that the solution may contain swaps, if the cost function is not appropriately designed (e.g. improperly chosen regularization parameter, organs with inner cavities). The proposed algorithm is fundamentally different from most of the current graph search methods, which are designed for equi-spaced nodes. Since the new formulation significantly reduces the graph layers compared to GOOSE, it provides an order of magnitude reduction in computational complexity and memory demand. Hence, the new algorithms are readily applicable to large-scale 3D fat-water imaging applications. Quantitative comparisons between GOOSE, R-GOOSE and mR-GOOSE were performed using datasets from 2012 ISMRM challenge.

Methods

Signal model and GOOSE formulation

In gradient echo acquisitions, the signal is collected in a succession of echo time (TE) shifts, t_1, $t_2, \ldots,$ t_N. At each location $\mathbf{r} = (x, y, z)$, it can be expressed as a combination of fat and water components. The

matrix form can be expressed as:

$$\underbrace{\begin{bmatrix} e^{-\gamma\, t_1} & e^{-\gamma\, t_1}\left(\sum_{i=1}^{M}\beta_i e^{j2\pi\delta_i\, t_1}\right) \\ .. & \\ e^{-\gamma\, t_n} & e^{-\gamma\, t_n}\left(\sum_{i=1}^{M}\beta_i e^{j2\pi\delta_i\, t_n}\right) \end{bmatrix}}_{\mathbf{A}_\gamma} \underbrace{\begin{bmatrix} \rho_{\text{water}} \\ \rho_{\text{fat}} \end{bmatrix}}_{\mathbf{g}} = \underbrace{\begin{bmatrix} s[1] \\ .. \\ s[N] \end{bmatrix}}_{\mathbf{s}}. \qquad [1]$$

In [1], the model contains one water peak and $\mathbf{M}$ fat peaks, each of which has a chemical shift δ_i to the water peak. $\rho_{\text{water}}, \rho_{\text{fat}}$ are the complex valued concentrations of water and fat and β_i denotes the relative weight of each peak. $\gamma(\mathbf{r}) = [1/T_2^*(\mathbf{r}) - j2\pi f(\mathbf{r})]$, represents the combined effect of the local frequency shift $f(\mathbf{r})$ due to the static field inhomogeneity and the T_2^* decay. Assuming that β_i and δ_i are known (21), the unknowns $\rho_{\text{water}}, \rho_{\text{fat}}$ and $\gamma(\mathbf{r})$ ($f(\mathbf{r})$ and T_2^*) at each voxel can be obtained by minimizing the least-square error between the model and the measured data $\|\mathbf{A}_\gamma\mathbf{g} - \mathbf{s}\|^2$. The estimation of T_2^* can be achieved through an independent search over a reasonable range of discrete T_2^* values (12). For a specific value of $f(\mathbf{r})$ and $T_2^*(\mathbf{r})$, the concentrations ρ_{water} and ρ_{fat} can be obtained as $\mathbf{g} = (\mathbf{A}_\gamma^T\mathbf{A}_\gamma)^{-1}\mathbf{A}_\gamma^T\mathbf{s}$. Substituting the optimal values for a specific frequency back, we obtain:

$$\hat{f}(\mathbf{r}) = \arg\min_{f(\mathbf{r})} \underbrace{\min_{\rho_{\text{water}},\rho_{\text{fat}},T_2^*} \|\mathbf{A}_\gamma\mathbf{g} - \mathbf{s}\|^2}_{\mathcal{D}(f(\mathbf{r}))} \qquad [2]$$

Here, $\mathcal{D}\left(f(\mathbf{r})\right)$ is the voxel independent maximum likelihood prior.

Since the voxel independent prior has multiple local minima at each location, the recovery of the field map at all pixels was formulated as a single optimization problem (19):

$$\begin{aligned} \hat{f} \;=\; & \arg\min_{f(\mathbf{r})} \sum_{\mathbf{r}} \mathcal{D}\left(f(\mathbf{r})\right) \quad \text{such that} \\ & |f(\mathbf{r}+\mathbf{e}_x) - f(\mathbf{r})| \le F \\ & |f(\mathbf{r}+\mathbf{e}_y) - f(\mathbf{r})| \le F. \end{aligned} \qquad [3]$$

Here, $\mathbf{e}_x = (1,0,0)$ and $\mathbf{e}_y = (0,1,0)$ are the unit vectors in the x and y directions. GOOSE imposes hard constraints for the permissible deviation of frequency values between adjacent voxels. To solve the above optimization problem, the frequency values are discretized onto a uniformly full grid with a grid spacing Δ,

where F is assumed to be a multiple of Δ. A brief graph illustration can be seen in Fig. 1.(a). The readers are referred to (19) for more details.

Proposed algorithm

The proposed formulation considers a non-uniform discretization of the frequency axis, compared to the uniform discretization strategy in GOOSE. In this work, each of the graph nodes at a specific voxel corresponds to a local minimum of $\mathcal{D}\left(f(\mathbf{r})\right)$, which belongs to the local minima set denoted by $\text{LM}(\mathbf{r})$ for each spatial location. Here, the optimization models in [2] and [3] are replaced by a smoothness penalized 3D optimization formulation for field map estimation:

$$\hat{f} = \arg\min_{f(\mathbf{r})} \sum_{\mathbf{r}} \left(\underbrace{\mathcal{D}(f(\mathbf{r}))}_{\text{data consistency}} + \mu \underbrace{\sum_{\mathbf{s}\in\mathcal{N}(\mathbf{r})} w_{\mathbf{rs}} |f(\mathbf{r}) - f(\mathbf{s})|^2}_{\text{smoothness regularization}} \right), \quad f(\mathbf{r}) \in \text{LM}(\mathbf{r}); \forall \mathbf{r} \qquad [4]$$

The term $\mathcal{N}(\mathbf{r})$ in [4] denotes the local neighborhood of the voxel at location $\mathbf{r}$. $w_{\mathbf{rs}}$ are pre-defined weights that penalize the differences between field map values in the neighborhood $\mathcal{N}(\mathbf{r})$ as in (12). The first term promotes the consistency between the data model and measurements and the second term encourages field map smoothness. μ is the regularization parameter that balances the first term and second term. The choices of $f(\mathbf{r})$ are limited to $\text{LM}(\mathbf{r})$, the set of minimizers at location $\mathbf{r}$.

R-GOOSE

We solve [4] using a single-step graph optimization algorithm. As shown in Fig.2, we start with the determination of the local minima $\text{LM}(\mathbf{r})$ by searching for the zero crossings of the derivatives of the voxel independent likelihood term $\mathcal{D}\left(f(\mathbf{r})\right)$; the derivatives are approximated by finite differences. We then build a graph in which nodes at each voxel correspond to the local minimize set $\text{LM}(\mathbf{r})$. The nodes of the graph are equispaced on a uniform space of size $N_x \times N_y \times N_z$, where N_x, N_y and N_z are the sizes in x, y and z directions, respectively. By contrast, the nodes are non-equispaced in frequency. We denote the number of discrete field map values at each location $\mathbf{r} = (x, y, z)$ as N_f. This is a key difference from the uniform graph assumed in GOOSE, where the field map values of the nodes are uniformly spaced with a frequency difference of Δ (See Fig.1.(a) and Fig.1.(b)).

Let $\mathrm{Col}(\mathbf{r})$ represent a column of N_f nodes at the spatial location $\mathbf{r} = (x, y, z)$, where $x \in [0, \ldots N_x - 1]$, $y \in [0, \ldots N_y - 1]$ and $z \in [0, \ldots N_z - 1]$. The frequency values of the N_f nodes in $\mathrm{Col}(\mathbf{r})$ are specified by the set $f(\mathbf{r}) \in \mathrm{LM}(\mathbf{r})$. Each node cost is specified by $\mathcal{D}\left(f(\mathbf{r})\right)$, where $f(\mathbf{r})$ is the frequency value of the node. In our formulation, a node in $\mathrm{Col}(\mathbf{r})$ is connected with all nodes in the adjacent column $\mathrm{Col}(\mathbf{s})$, provided $\mathbf{s}$ is in the neighborhood of $\mathbf{r}$ (i.e., $\mathbf{s} \in \mathcal{N}(\mathbf{r})$). The smoothness cost between the i^{th} node in $\mathrm{Col}(\mathbf{r})$ and j^{th} node in $\mathrm{Col}(\mathbf{s})$ is specified by $\mu\, w_{\mathbf{r},\mathbf{s}} \left|f_i(\mathbf{r}) - f_j(\mathbf{s})\right|^2$. This is another key difference with the graph construction in GOOSE, where each node was only allowed to connect with a subset of nodes in the adjacent column specified by the smoothness constraint. With the new graph construction, solving Eq.[4] translates into a surface estimation problem. We seek to find a surface $S(\mathbf{r}) = \hat{f}(\mathbf{r})$ that intersects with only one node in each column and the sum of node costs and smoothness costs are minimized.

We search for the optimal surface using the algorithm introduced in (22), which is designed for graphs with non-uniform spacings. Since the smoothness penalty involves a convex (quadratic in our setting) distance measure, the graph algorithm (22) is guaranteed to converge to the global minimum of Eq.[4]. The readers are referred to (22) for details.

mR-GOOSE

Since R-GOOSE ensures convergence to the global minimum as shown in (22), we only use multi-resolution strategies to further reduce the computation complexity. We first subsample $\mathcal{D}(\mathbf{r})$ along the spatial dimensions to obtain the data consistency prior at each low-resolution pixel, which is the sum of $\mathcal{D}(\mathbf{r})$ from the corresponding square pixel neighborhood in the high-resolution volume. The downsampling factor is the length of a side of the square neighborhood. An example of the downsampling process is shown in the Sup. Fig. S1, where the data consistency prior at the low-resolution pixel obtained from a 2 by 2 neighborhood in the original volume of $\mathcal{D}(\mathbf{r})$. Here, the downsampling factor is 2. After the local minima set $\mathrm{LM}(\mathbf{r})$ in low resolution is identified, the graph search algorithm is executed to determine the coarse estimate of the field map.

In the refinement step, the above coarse estimate is interpolated onto the finer grid. Specifically, the set $\mathrm{LM}(\mathbf{r})$ in the original resolution is formed by only selecting the minimizers closest to the coarse scale estimate. In our implementation, we only selected two local minima at each pixel in the original-resolution dataset, which are the closest to the interpolated coarse scale estimate. A graph with only two layers in the second search leads to a further reduction of computation time. The refinement steps are also shown in the

Sup. Fig. S1.

Experiments and Parameters

In this work, results of the 17 datasets from 2012 ISMRM Challenge by applying the R-GOOSE and mR-GOOSE frameworks are compared against those from GOOSE in quantitative accuracy and computation time. The quantitative accuracy, or the score is determined by the percentage of pixels in the pre-defined mask in which the difference of fat fraction between the tested result and the reference is less than a threshold (0.1). Details can be found at the ISMRM Challenge website (`http://www.ismrm.org/challenge/`). We adopt the parameters of the reference signal model in the judging section of the 2012 ISMRM Challenge. Specifically, we use six fat spectral peaks at δ_i = [-242.7060, -217.1580, -166.0620, -123.9078, -24.9093, 38.3220] Hz at 1.5T, with relative weights β_i = [0.0870, 0.6930, 0.1280, 0.0040, 0.0390, 0.0480]. A single T_2^* constant is used at each voxel. The search of $1/T_2^* = R_2^*$ is separated as a preprocessing step before field map estimation, and is repeated with the obtained field map after graph search for optimization. All algorithms are computed on the Linux Workstation with 3.2 GHz Intel Xeon CPU and 23.6GB RAM.

Three parameters need to be optimized in the proposed algorithm: 1) N_f, the number of graph layers, or the number of entries in LM . N_f should be able to cover the field inhomogeneity range which can be estimated by $1/\Delta\text{TE}$ for uniformly sampled data. $\mathcal{D}(f(\mathbf{r}))$ is periodic and contains at least two minimizers in each period in a typical case with both fat and water for the pixel. The largest range of field inhomogeneity for all the 17 datasets is about $[0, 1020]$Hz in dataset 12 and contains up to 5 periods (about 12 minimizers). Therefore, we test $N_f = 3$ up to 12 to ensure the coverage of the entire field inhomogeneity. 2) N_r, the number of discrete values of R_2^*. We use the search range of R_2^* as $0\,\text{s}^{-1}$ to $500\,\text{s}^{-1}$ with the number of discrete values $N_r = [2, 10, 20, 30, 40, 50, 60, 70, 80]$. 3) μ, the regularization parameter in Eq.[4]. Similar to (12) and (15), the optimization is conducted in the range of $[0.01, 100]$.

Optimal parameters are determined by applying R-GOOSE with the above-mentioned different values and benchmarking the quantitative scores with the reference in the first four uniformly sampled datasets. Note that the proposed framework can still be applied to non-uniformly sampled dataset such as dataset 3. Since the pattern of $\mathcal{D}(f(\mathbf{r}))$ for the non-uniformly sampled data is different from the uniformly sampled data, dataset 3 is not used to optimize N_f for the rest of uniformly sampled datasets in this experiment.

RESULTS

Parameter Optimization

The study of N_f with respect to the average score is shown in Fig.3(a). The average score starts to plateau around 9980 for R-GOOSE when $N_f = 8$. A better quantitative performance as N_f increases is because the field variation is not fully accounted for until $N_f = 8$. In Fig.3(b), the average score reaches the maximum around 9980 when N_r is larger than 30. Therefore, we chose $N_r = 30$ for the rest of the study. The average scores remain relatively unchanged between $\mu = 0.1$ and $\mu = 10$ in Fig.3(c). μ is set as 0.5 for the rest of experiments with the highest performance. The average run-time increases as the number of N_f goes bigger as in Fig.3.(d).

Comparison with GOOSE

In Fig.4, the liver dataset is challenging because the dome of the liver is surrounded by a signal void at the 2nd slice. This large low SNR region results in a swap in GOOSE and other state-of-the-art algorithms (See (19) Fig.7). In GOOSE, the difference between adjacent field map values is strictly set to be less than the hard constraint F in Eq.[3]. However, the soft constraint as the smoothness penalty term in Eq.[4] in the proposed formulation permits a necessary 'jump' of field map from one node to its next. Both R-GOOSE and mR-GOOSE successfully resolve the fat water swap as pointed by the arrow in the figure. The proposed method employs a three-dimensional graph search scheme that also takes into account the field map smoothness across slices. For example, we were not able to correct the fat-water swap in one slice of a breast dataset in GOOSE, whereas the separation is correct on all slices using R-GOOSE. Results can be seen in Sup. Fig. S2.

Table 1 shows quantitative scores and run-times from GOOSE (G), R-GOOSE (RG) and mR-GOOSE (mRG, with a downsampling factor of 4) across the 17 datasets. Both R-GOOSE and mR-GOOSE obtain higher scores than GOOSE over the 17 datasets. The average run-time is 323 seconds for GOOSE while it is 8.1 for R-GOOSE on average and 4.5 for mR-GOOSE. The new graph construction with the non-uniform spacing effectively mitigates this discretization error while also reducing the computational complexity in GOOSE.

DISCUSSION & CONCLUSION

As an extension of GOOSE, this paper introduced a new graph search model for efficiently solving 3D fat-water separation problem. The new graph model enables the existence of non-uniform spacing between nodes, reducing the number of graph layers in GOOSE by an order of magnitude (10-12 layers). Since the nodes are non-uniformly spaced, a novel graph based surface estimation method (22) is introduced to solve the optimization problem. This gives rise to a significant reduction in graph connectivity. The employment of non-uniformly spaced nodes and the new graph construction result in faster computation and lower memory demand than GOOSE.

Meanwhile, the proposed approach incorporates a smoothness term which penalizes the difference between two neighboring solutions using a quadratic penalty. Since we restrict the solutions to the local minima at each location, the algorithm is also robust to the selection of the smoothness regularization parameter. The restriction of graph search to local minima also improves the accuracy of fat-water recovery compared to GOOSE. In particular, R-GOOSE and mR-GOOSE achieve full score in dataset 9 and 13. This is possible because the proposed method only chooses solutions from the exact minimizers, whereas GOOSE also considers possible field map values in the vicinity of the minimizers. In our experiment, the separation results are observed to be consistant and stable once the number of local minima N_f is larger than 8 at each location. With the high accuracy and reduced run-time, both R-GOOSE and mR-GOOSE can be potentially used in different applications such as Quantitative Susceptibility Mapping (QSM). R-GOOSE or mR-GOOSE can be considered as an alternative to the current phase unwrapping procedure and the field inhomogeneity removal, through which a more accurate QSM can be obtained.

This smoothness-penalized optimization formulation in [4] is identical to (12). The main difference here is the restriction of the feasible solutions at each pixel to the set $\mathrm{LM}(\mathbf{r})$. A similar strategy was used in (15), where the solutions are restricted to two local minima at each pixel. Since the quadratic pseudo boolean optimization (QPBO) algorithm in (15, 23) can only yield a partial solution, iterated conditional modes (ICM) (23) or multi-scale optimization was used (15) to ensure global convergence. However, we rely on a single-step algorithm (R-GOOSE) with guarantee of convergence to the global optimum of the cost function. The results of R-GOOSE and mR-GOOSE are comparable and multi-scale scheme (mR-GOOSE) is solely to reduce the run-time.

As we note in Introduction, though GOOSE, R-GOOSE and mR-GOOSE benefit from the global opti-

mality of cost functions to achieve high performance without an iterative process, the global convergence property alone will not guarantee the correct separation of water and fat, particularly in challenging datasets. Like all methods that rely on optimization, the cost function needs to be designed and optimized carefully to ensure that the global minimizers are free of fat-water swaps. The benefit of the proposed formulation is that the proposed scheme does not require additional steps to ensure global convergence and is not sensitive to initialization in many iterative methods.With the global convergence guarantee, the proposed algorithm is an excellent tool to improve the formulation of the energy function.

Though the proposed work has significantly reduced the memory demand for graph construction (100 layers to 9 layers per slice on average), one limitation of the proposed work is the memory requirement for hardware in solving large 3D cases. In order to perform a globally optimal search, the graph search method, by nature, is designed to include all entries of the set $\mathrm{LM}(\mathbf{r})$ at each pixel and the associated edge connectivity in the neighborhood of the pixel. With the edge connectivity among slices, the constructed 4D graph volume (3 spatial dimensions plus a 4th frequency dimension) will need larger memory storage than the summation of the 3D graph volumes at each slice. Therefore, a certain assessment for hardware capacity might be taken into account before the proposed method is applied on very large 3D datasets. One possible workaround is to reduce the size of $\mathrm{LM}(\mathbf{r})$ by only keeping entries with smallest data costs $\mathcal{D}(f(\mathbf{r}))$. This can be achieved by using techniques such as thresholding the data costs among all minimizers at each location.

In conclusion, a non-equidistant graph search model is proposed in this work to improve the fully discretized model in our previous work GOOSE. Both frameworks, R-GOOSE and mR-GOOSE achieve high accuracy for fat water separation in ISMRM Challenge datasets, while the computation time is reduced by an order of magnitude compared to GOOSE.

ACKNOWLEDGEMENT

The authors would like to thank the organizers and developers of the ISMRM fat water toolbox, which was used for the comparisons in this paper (http://ismrm.org/workshops/FatWater12/data.htm). The authors would also like to thank the committee of 2012 ISMRM Challenge for providing data and codes to test our algorithm (http://www.ismrm.org/challenge/). The authors also thank the anonymous reviewers, whose insightful comments considerably improved the quality of the manuscript. The implementation of the pro-

posed algorithm can be found at https://research.engineering.uiowa.edu/cbig/content/r-goose.

Legends

Figure. 1Illustration of the graph constructions in GOOSE (a) and R-GOOSE (b). For simplicity, we restrict our attention to 2D graphs, while our implementation is in 4D. The maximum likelihood measurement specified by $\mathcal{D}(f(\mathbf{r}))$ is discretized on a uniform grid of field map values; the plot of $\mathcal{D}(f(\mathbf{r}))$ at a specific pixel is shown in (c). (a) In GOOSE, the fieldmap was uniformly discretized with each node corresponding to a discrete frequency, indicated by the black dotted lines in (c) and the black circles in (a) and (c). A graph smoothness constraint was used in GOOSE, where each node was connected to only $(2\alpha + 1)$ nearby nodes in the adjacent pixels. Here, the smoothness constraint α is 1. The node costs were chosen as $\mathcal{D}(f(\mathbf{r}))$, while no smoothness costs were considered. (b) In R-GOOSE, we only consider the local minimizers of $\mathcal{D}(f(\mathbf{r}))$, which correspond to the nodes at each voxel, indicated by the green circles in (b) and (c). Note that the nodes are not equispaced in the R-GOOSE setting. We use a graph smoothness penalty in R-GOOSE as opposed to the smoothness constraint in GOOSE. Hence, each node in a pixel is connected to all the nodes in the adjacent pixels. The node costs are still chosen as $\mathcal{D}(f(\mathbf{r}))$, while the smoothness cost between the i^{th} node in pixel $\mathbf{r}$ and the j^{th} node in its neighboring pixel $\mathbf{s}$ are chosen as $w_{\mathbf{r},\mathbf{s}}|f_i - f_j|^2$.The objective here is to find the surface (S) that minimizes the total of both costs.

Figure. 2 The information flow in the implementation of R-GOOSE. We discretize $\mathcal{D}(f(\mathbf{r}))$ in Eq.[4] on a uniform grid. Then we extract all minimizers (colorcoded in green) using finite difference method and import them to the graph model. The field map and the initial $R_2^* = 1/T_2^*$ map are obtained after the globally optimal surface estimation using the proposed smoothness penalized optimization formulation. The R_2^* is then updated in refinement using field map from graph search, which in conjunction with the field map is used for estimating fat water concentrations. The fat and water recovery can be achieved in steps after Graph Search.

Figure. 3 Dependence of the solution on the parameters. In (a), the change of the average score as a function of the number of layers (minimizers) N_f at 3 to 12 is plotted. The overall performance of R-GOOSE reaches the similar level as GOOSE (the dash line) when $N_f = 9$. (b) is the plot for the average scores obtained from R-GOOSE as a function of the number of R_2^* points, N_r. Here, we use $N_f = 9$ and $\mu = 100$. We choose $N_r = 30$ for the rest of the experiments. N_r is observed to have little impact on computation time

so the result of the time change with respect to N_r is not shown here. The score change with respect to the penalty parameter μ is shown in (c) for R-GOOSE. The scores are consistent across all N_f when μ is between [0.1, 2.0]. (d) is the plot for the relation between the average use of time and N_f. The average time of $N_f = 8$ is around 8 seconds and is reduced by an order of magnitude overall compared to GOOSE, the dash line in the figure. Together with (a), we can see that R-GOOSE is able to achieve the same level of accuracy with at least 30 times of time saving in comparison with GOOSE.

Figure. 4 Qualitative comparisons between GOOSE, R-GOOSE, and mR-GOOSE on a liver dataset (2012 Challenge dataset 12). The fat fraction map shows that both R-GOOSE and mR-GOOSE resolve the swap while it remains in the the result from GOOSE. Overall, the proposed methods outperform GOOSE by more than 6% in quantitative scoring.

Table. 1 Quantitative scores and computational time comparisons of the proposed scheme against GOOSE. The first three rows are quantitative scores of GOOSE (Q(G)), R-GOOSE (Q(RG)) and mR-GOOSE (Q(mRG)) for the 17 datasets. The last three rows are the computational time in seconds of graph search for GOOSE (T(G)), R-GOOSE (T(RG)) and mR-GOOSE (Q(mRG))). Note that the scores of GOOSE are the average of scores of multiple 2D single slices processed using GOOSE.

Supporting Figure S1. The information flow in the implementation of mR-GOOSE. In the multi-resolution frame, the new downsampled $\mathcal{D}(f(\mathbf{r}))$ is computed as a summation of the local patch of the original data consistency. Once the initial field map is acquired from graph search, the set of minimizers is chosen to be the two candidates closest in frequency to the initial coarse estimate at each location. Then the final field map is refined by running the graph search for the second time. The fat and water recovery can be achieved in steps after Graph Search.

Supporting Figure S2. Qualitative comparisons between GOOSE and R-GOOSE on a breast dataset (2012 Challenge dataset 15). Since the proposed method incorporates the inter-slice correlation in the 3D graph surface search, the proposed method is able to correct a fat-water swap that occurs in GOOSE as pointed by arrows.

References

1 Bley TA, Wieben O, François CJ, Brittain JH, and Reeder SB. Fat and water magnetic resonance imaging. J Magn Reson, 2010; 31:4–18.

2 Hu HH, Kim H, Nayak KS, and Goran MI. Comparison of Fat–Water MRI and Single-voxel MRS in the Assessment of Hepatic and Pancreatic Fat Fractions in Humans. Obesity, 2010; 18:841–847.

3 Reeder SB, Robson PM, Yu H, Shimakawa A, Hines CDG, McKenzie CA, and Brittain JH. Quantification of hepatic steatosis with MRI: the effects of accurate fat spectral modeling. J Magn Reson, 2009; 29:1332–1339.

4 Haase A, Frahm J, Hanicke W, and Matthaei D. 1H NMR chemical shift selective (CHESS) imaging. Physics in Medicine and Biology, 2000; 30:341.

5 Meyer CH, Pauly JM, Macovski A, and Nishimura DG. Simultaneous spatial and spectral selective excitation. Magn Reson Med, 2005; 15:287–304.

6 Dixon WT. Simple proton spectroscopic imaging. Radiology, 1984; 153:189–194.

7 Glover G and Schneider E. Three-point dixon technique for true water/fat decomposition with b0 inhomogeneity correction. Magnetic resonance in medicine, 1991; 18:371–383.

8 Reeder SB, Wen Z, Yu H, Pineda AR, Gold GE, Markl M, and Pelc NJ. Multicoil dixon chemical species separation with an iterative least-squares estimation method. Magnetic Resonance in Medicine, 2004; 51:35–45.

9 Yu H, Reeder SB, Shimakawa A, Brittain JH, and Pelc NJ. Field map estimation with a region growing scheme for iterative 3-point water-fat decomposition. Magn Reson Med, 2005; 54:1032–1039.

10 Berglund J, Johansson L, Ahlstrom H, and Kullberg J. Three-point Dixon method enables whole-body water and fat imaging of obese subjects. Magn Reson Med, 2010; 63:1659–1668.

11 Jacob M and Sutton BP. Algebraic decomposition of fat and water in MRI. IEEE Trans Med Imaging, 2009; 28:173–184.

12 Hernando D, Kellman P, Haldar JP, and Liang ZP. Robust water/fat separation in the presence of large field inhomogeneities using a graph cut algorithm. Magn Reson Med, 2010; 63:79–90.

13 Lu W and Hargreaves BA. Multiresolution field map estimation using golden section search for water-fat separation. Magn Reson Med, 2008; 60:236–244.

14 Tsao J and Jiang Y. Hierarchical IDEAL: Fast, robust, and multiresolution separation of multiple chemical species from multiple echo times. Magn Reson Med, 2012; 70:155–159.

15 Berglund J and Skorpil M. Multi-scale graph-cut algorithm for efficient water-fat separation. Magnetic Resonance in Medicine, 2016.

16 Cheng C, Zou C, Liang C, Liu X, and Zheng H. Fat-water separation using a region-growing algorithm with self-feeding phasor estimation. Magnetic Resonance in Medicine, 2016. ISSN 1522-2594. doi: 10.1002/mrm.26297. URL `http://dx.doi.org/10.1002/mrm.26297`.

17 Soliman AS, Yuan J, Vigen KK, White JA, Peters TM, and McKenzie CA. Max-ideal: A max-flow based approach for ideal water/fat separation. Magnetic resonance in medicine, 2014; 72:510–521.

18 Liu J and Drangova M. Method for b0 off-resonance mapping by non-iterative correction of phase-errors (b0-nice). Magnetic resonance in medicine, 2015; 74:1177–1188.

19 Cui C, Wu X, Newell JD, and Jacob M. Fat water decomposition using globally optimal surface estimation (goose) algorithm. Magn Reson Med, 2015; 73:1289–1299.

20 Wu X and Chen D. Optimal net surface problems with applications. Automata, Languages and Programming, 2002; 2380:1029–1042.

21 Yu H, Shimakawa A, McKenzie CA, Brodsky E, Brittain JH, and Reeder SB. Multiecho water-fat separation and simultaneous R2* estimation with multifrequency fat spectrum modeling. Magn Reson Med, 2008; 60:1122–1134.

22 Shah A, Bai J, Abramoff MD, and Wu X. Optimal multiple surface segmentation with convex priors in irregularly sampled space. arXiv preprint arXiv:1611.03059, 2016.

23 Berglund J and Kullberg J. Three-dimensional water/fat separation and t2* estimation based on whole-image optimizationapplication in breathhold liver imaging at 1.5 t. Magnetic Resonance in Medicine,

2012; 67:1684–1693. ISSN 1522-2594. doi: 10.1002/mrm.23185. URL http://dx.doi.org/10.1002/mrm.23185.

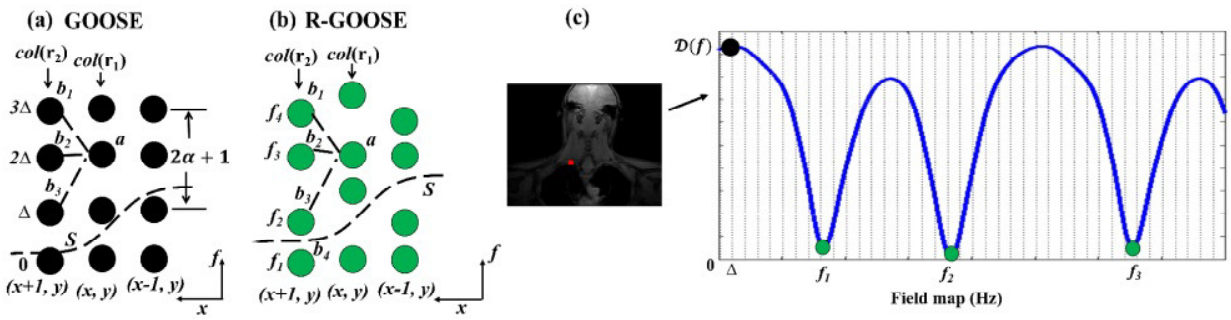

Figure 1: Illustration of the graph constructions in GOOSE (a) and R-GOOSE (b). For simplicity, we restrict our attention to 2D graphs, while our implementation is in 4D. The maximum likelihood measurement specified by $\mathcal{D}(f(\mathbf{r}))$ is discretized on a uniform grid of field map values; the plot of $\mathcal{D}(f(\mathbf{r}))$ at a specific pixel is shown in (c). (a) In GOOSE, the fieldmap was uniformly discretized with each node corresponding to a discrete frequency, indicated by the black dotted lines in (c) and the black circles in (a) and (c). A graph smoothness constraint was used in GOOSE, where each node is connected to only $(2\alpha + 1)$ nearby nodes in the adjacent pixels. Here, the smoothness constraint α was 1. The node costs were chosen as $\mathcal{D}(f(\mathbf{r}))$, while no smoothness costs were considered. (b) In R-GOOSE, we only consider the local minimizers of $\mathcal{D}(f(\mathbf{r}))$, which correspond to the nodes at each pixel, indicated by the green circles in (b) and (c). Note that the nodes are not equispaced in the R-GOOSE setting. We use a graph ssmoothness penalty in R-GOOSE as opposed to the smoothness constraint in GOOSE. Hence, each node in a pixel is connected to all the nodes in the adjacent pixels. The node costs are still chosen as $\mathcal{D}(f(\mathbf{r}))$, while the smoothness cost between the i^{th} node in pixel $\mathbf{r}$ and the j^{th} node in its neighboring pixel $\mathbf{s}$ are chosen as $w_{\mathbf{r},\mathbf{s}}|f_i - f_j|^2$.The objective here is to find the surface (S) that minimizes the total of both costs.

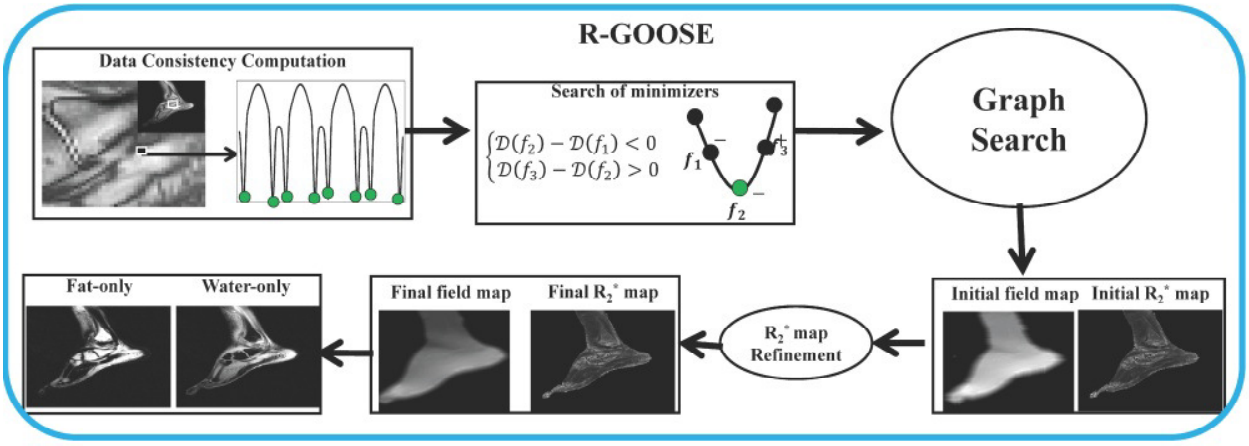

Figure 2: The information flow in the implementation of R-GOOSE. We discretize $\mathcal{D}(f(\mathbf{r}))$ in Eq.[4] on a uniform grid. Then we extract all minimizers (colorcoded in green) using finite difference method and import them to the graph model. The field map and the initial $R_2^* = 1/T_2^*$ map are obtained after the globally optimal surface estimation using the proposed smoothness penalized optimization formulation. The R_2^* is then updated in refinement using field map from graph search, which in conjunction with the field map is used for estimating fat water concentrations. The fat and water recovery can be achieved in steps after Graph Search.

Method	Mean	1	2	3	4	5	6	7	8	9	10	11	12	13	14	15	16	17
Q(G)	99.27	99.84	99.81	96.50	99.87	99.94	99.88	99.90	99.94	99.97	99.72	99.75	95.58	99.91	99.87	99.15	99.13	98.80
Q(RG)	99.39	99.83	99.81	95.95	99.90	99.99	99.79	99.91	99.95	100.00	99.73	99.61	97.63	100.00	99.71	99.52	99.57	98.75
Q(mRG)	99.46	99.84	99.83	96.12	99.89	100.00	99.87	99.91	100.00	100.00	99.88	99.79	97.75	100	99.72	99.69	99.67	98.93
T(G)	323.9	220.7	183.5	269.2	319.1	318.8	160.8	314.4	700.9	829.3	224.9	536.7	522.4	192.4	422.7	76.7	154.8	59.4
T(RG)	8.1	9.1	8.3	9.1	10.5	14.5	10.9	10.6	9.4	7.1	8.9	4.2	10.2	2.3	9.5	7.4	2.7	3.5
T(mRG)	4.5	4.2	4.8	3.6	5.1	5.5	5.0	5.8	3.6	4.6	4.7	5.6	4.9	2.7	5.0	4.8	3.3	3.2

Table 1: Quantitative scores and computational time comparisons of the proposed scheme against GOOSE. The first three rows are quantitative scores of GOOSE (Q(G)), R-GOOSE (Q(RG)) and mR-GOOSE (Q(mRG)) for the 17 datasets. The last three rows are the computational time in seconds of graph search for GOOSE (T(G)), R-GOOSE (T(RG)) and mR-GOOSE (Q(mRG)). Note that the scores of GOOSE are the average of scores of multiple 2D single slices processed using GOOSE.

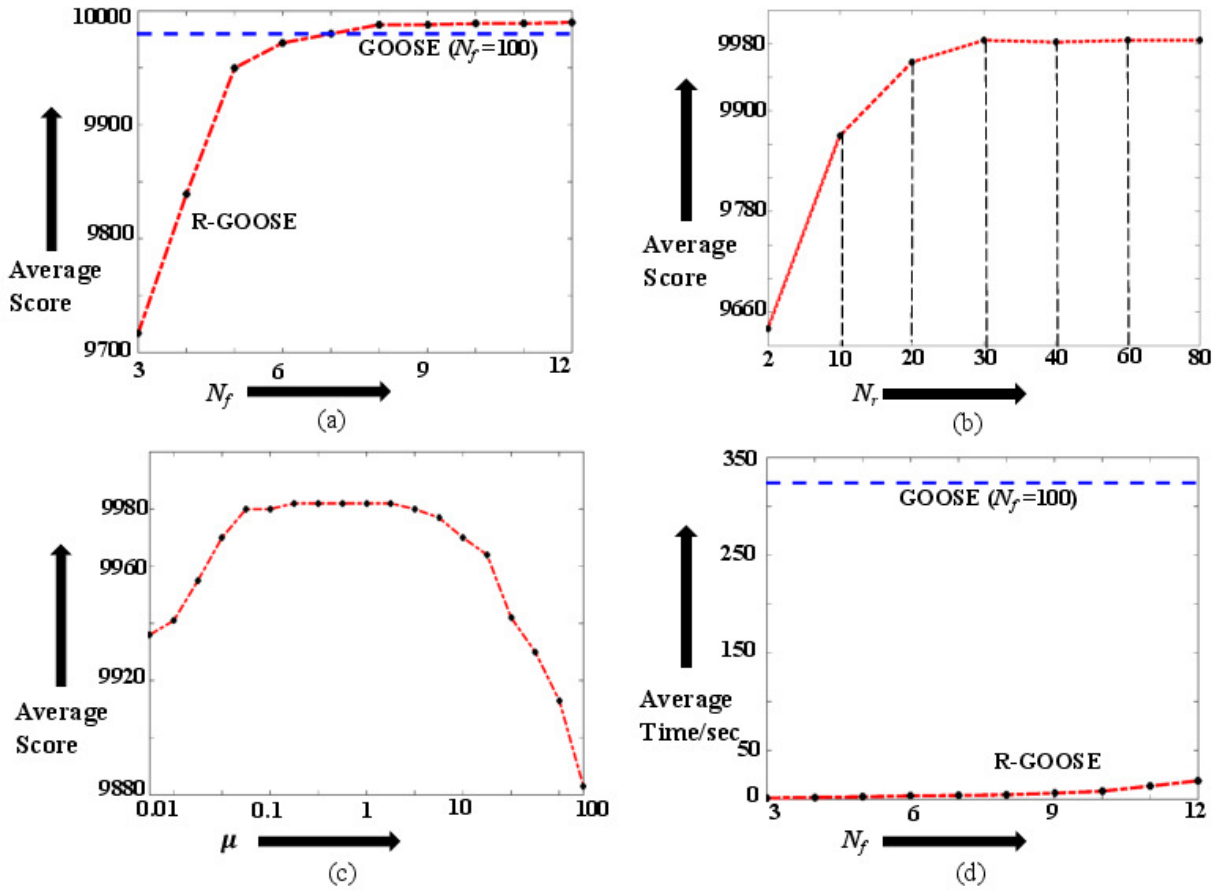

Figure 3: Dependence of the solution on the parameters. In (a), the change of the average score as a function of the number of layers (minimizers) N_f at 3 to 12 is plotted. The overall performance of R-GOOSE reaches the similar level as GOOSE (the dash line) when $N_f = 9$. (b) is the plot for the averages score obtained from R-GOOSE as a function of the number of R_2^* points, N_r. Here, we use $N_f = 9$ and $\mu = 100$. We choose $N_r = 30$ for the rest of the experiments. N_r is observed to have little impact on computational time so the result of the time change with respect to N_r is not shown here. The score change with respect to the penalty parameter μ is shown in (c) for R-GOOSE. The scores are consistent across all N_f when μ is between [0.1, 2.0]. (d) is the plot for the relation between the average use of time and N_f. The average time of $N_f = 8$ is around 8 seconds and is reduced by an order of magnitude overall compared to GOOSE, the dash line in the figure. Together with (a), we can see that R-GOOSE is able to achieve the same level of accuracy with at least 30 times of time saving in comparison with GOOSE.

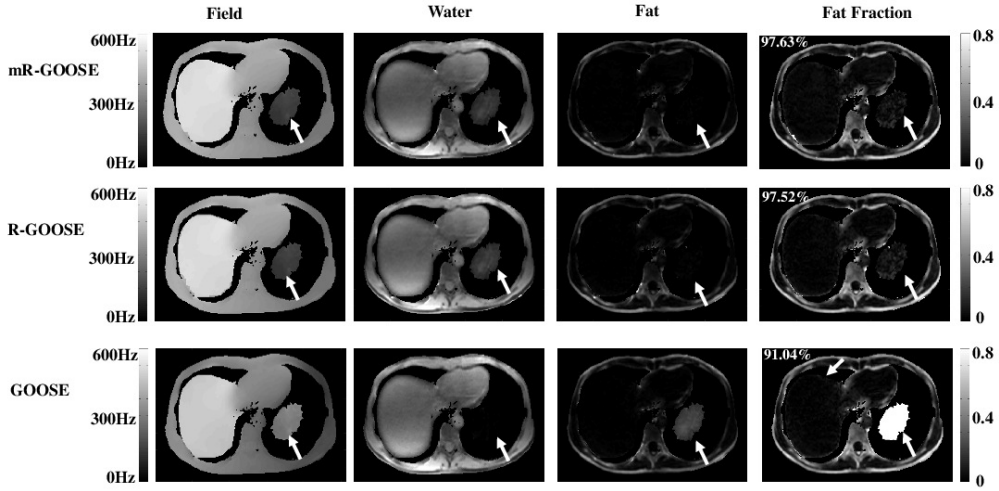

Figure 4: Qualitative comparisons between GOOSE, R-GOOSE, and mR-GOOSE on a liver dataset (2012 Challenge dataset 12). The fat fraction map shows that both R-GOOSE and mR-GOOSE resolve the swap while it remains in the the result from GOOSE. Overall, the proposed methods outperform GOOSE by more than 6% in quantitative scoring.

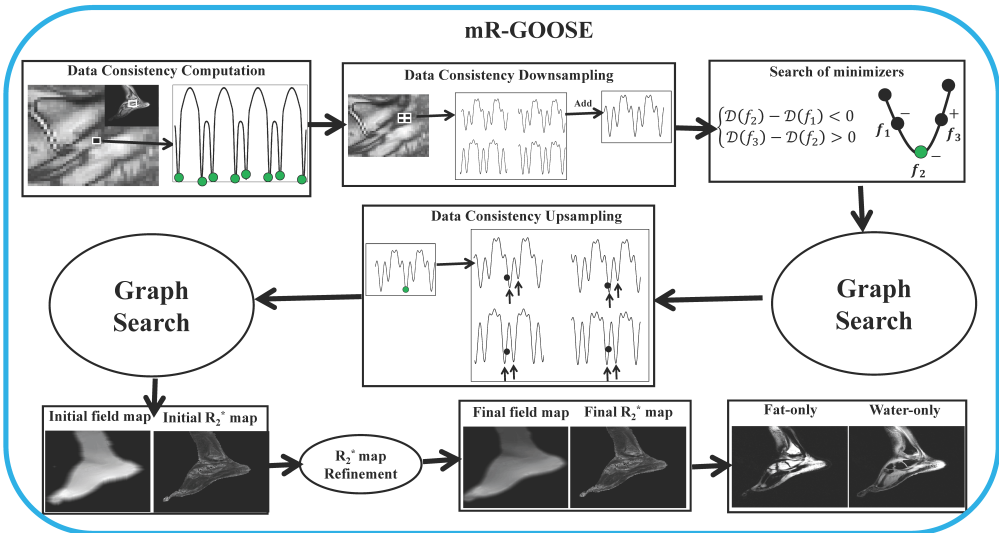

Supporting Figure S1. The information flow in the implementation of mR-GOOSE. In the multi-resolution frame, the new downsampled $\mathcal{D}(f(\mathbf{r}))$ is computed as a summation of the local patch of the original data consistency. Once the initial field map is acquired from graph search, the set of minimizers is chosen to be the two candidates closest in frequency to the initial coarse estimate at each location. Then the final field map is refined by running the graph search for the second time. The fat and water recovery can be achieved in steps after Graph Search.

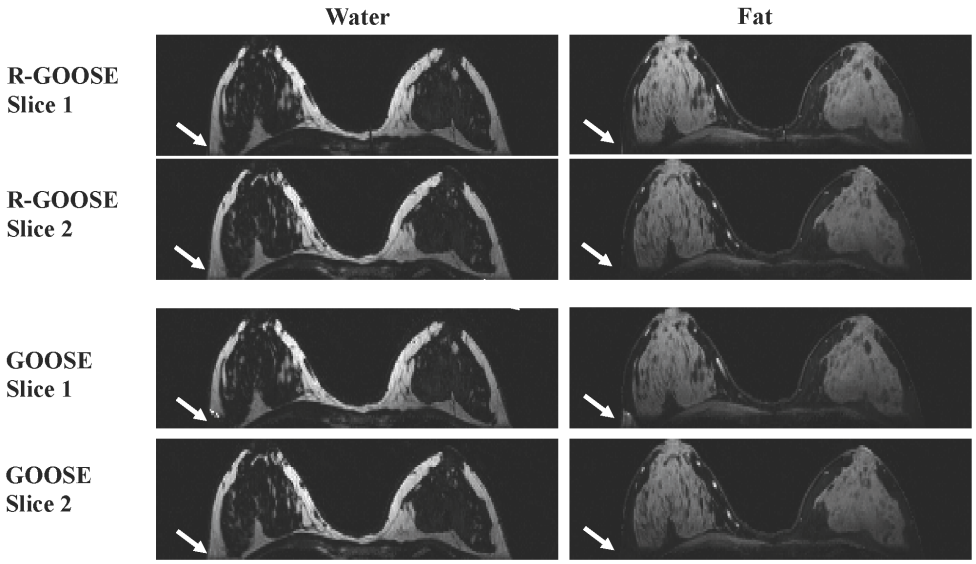

Supporting Figure S2. Qualitative comparisons between GOOSE and R-GOOSE on a breast dataset (2012 Challenge dataset 15). Since the proposed method incorporates the inter-slice correlation in the 3D graph surface search, the proposed method is able to correct a fat-water swap that occurs in GOOSE as pointed by arrows.